Optical hysteresis in laser-induced liquid-liquid phase separation

J. P. Delville, E. Freysz, and A. Ducasse
Centre de Physique Moléculaire Optique et Hertzienne, URA CNRS 283 UFR Physique, Université Bordeaux I, 351 Cours de la Libération, F-33405 Talence Cedex, France
(Received 13 March 1995)

We propose a method to obtain real hysteretical behavior in the optical area, and we analyze theoretically and experimentally its characteristics. This experimental method involves laser-induced electrostrictive and thermodiffusive concentration variations in order to drive a first-order phase transition in a liquid mixture. During the phase separation, generated droplets constituted by the minority phase are trapped in the laser beam. They behave as a set of optically coupled bistable spherical lenses that self-focus the wave. These changes in the optical properties of the medium result in a hysteretical behavior that can be interpreted from common general requirements of hysteretical systems. The difference between hysteresis and classical intrinsic optical bistability is discussed, and an analogy with the magnetization processes in ferromagnets is developed. The optical hysteresis is predicted from the Preisach model, and the shape of the hysteresis loops is quantitatively analyzed. We have also experimentally investigated specific behaviors of hysteretical systems, such as the asymptotic loop and cycle creep phenomena, which are often discarded and difficult to clearly observe and analyze.

PACS number(s): 64.70.Ja, 82.70.Kj, 75.60.Ej, 42.65.Jx

I. INTRODUCTION

Laser wave propagation through certain materials can be characterized by a bistable behavior even in the absence of any external feedback. This intrinsic optical bistability has aroused a great deal of interest over the last decade owing to its large application domain as a central point in switching devices. In such systems, the feedback mechanism results from the internal properties of the material and more precisely, from modifications induced by the exciting wave on its optical characteristics. Miller [1] developed a theoretical description of this process and showed its universality by indicating that intrinsic optical bistability originates from the coexistence of two nonequilibrium states characterized by different optical properties. This situation occurs for any first-order phase transition. It has been investigated theoretically [2] as well as experimentally [3] in the case of laser-induced phase transition between two phases of different absorptions. However, in these descriptions, neither the dynamic aspect of the phase transition nor the existence of metastable states was taken into account. Implicitly assumed was an idealized situation of first-order transitions in which precursor fluctuations were absent. As soon as one of the phases becomes thermodynamically unfavorable, it instantaneously transforms into the other phase. Although this picture is fairly realistic in some cases, there are situations where the metastable phase decay is impeded by some kinetics or mechanical constraints. In these cases, the spatial and temporal coexistence of high and low absorption domains is possible, and an amazing contrast with idealized first-order transitions is obtained. Thus, when the medium transforms from one phase to another without any sharp transition, hysteresis becomes the key phenomenon. Even if such domain formation has been suggested [4] and observed [5] in intrinsic optical bistability experiments, no attempt at interpretation in terms of optical hysteresis and no specific experiment has so far been reported. Two arguments can be suggested to explain this deficiency. First, optical hysteresis is, from a technical point of view, less common than optical bistability. Moreover, there is in the optical community a usual confusion between purely deterministic optical bistability and optical hysteresis. This leads to erroneously assimilating one process with the other. As a consequence, a better understanding of intrinsic optical memory effects needs fundamental analysis leading to a clear-cut distinction between the two manifestations.

In this paper we focus our attention on the difference between intrinsic optical bistability and hysteresis, and we quantitatively describe an experiment which allows us to study the optical hysteresis resulting from a first-order phase transition induced by a cw laser wave.

In fact, this difference was first proposed for magnetic hysteresis, almost 60 years ago, by Preisach [6]. In this model, which was based on some assumptions concerning the complicated physical mechanisms of magnetization, a ferromagnet is envisaged as a set of elementary domains with rectangular magnetization loops of varying coercivities. Hysteresis originates from this set of coupled bistable elements. This was further illustrated in a wide variety of physical systems, including fluid invasion of porous beds [7], martensitic transformations [8], and capillary condensation [9].

The present study develops these ideas in the optical area, in order to show that optical hysteresis exists and can be described with analogous arguments. In our case, hysteresis results from a mechanism of well-controlled laser-induced first-order phase transition in a binary liquid mixture, via wave-generated local variations of the concentration of one of the mixture components. Different processes of wave-medium coupling can be re-

sponsible for these induced composition variations in liquid mixtures. In recent years, it has been demonstrated that a thermal gradient gives rise to a concentration gradient via a thermodiffusive coupling [10]. Moreover, electrostriction, which results from dipolar forces induced by the wave, can also generate variations of composition [11]. Using micellar phases of microemulsions as particular mixtures, it has been previously demonstrated by self-focusing [12] and degenerate four-wave mixing [13] experiments that both thermodiffusion and electrostriction can be responsible for sizable concentration variations. These variations are sufficiently large to induce in a well-chosen sample a quench in composition resulting in a local phase separation [14]. Thus, inside the laser beam, droplets constituted by the minority phase can be nucleated in the initial one. In our particular case, their refraction index is larger than that of the majority phase. Then, owing to their large positive polarizabilities, they are trapped on the beam axis by electrostriction. In turn, these droplets behave as spherical lenses and self-focus the laser beam. Since the transition is first order, the van der Waals isothermas have an S-shaped structure and each droplet intrinsically behaves as a bistable optical element. Moreover, the associated lensing modifies the field distribution and induces optical couplings between the droplets. In other words, the optical response of the medium is the result of a beam propagation in a self-induced set of coupled bistable elements. Therefore, according to the mathematical description of the Preisach model [15], a hysteretical beam self-focusing is expected.

Our experiment allows a quantitative analysis of this expected optical hysteresis in a very simple geometry since it involves a quasi-one-dimensional pattern of nucleated droplets, equivalent to a string of coupled bistable elements. To study this behavior and to explore to what extent different hysteretical systems share universal features, we make an analogy with the magnetization processes in bulk ferromagnets. We show how the optical response due to the medium modifications can be macroscopically described from common general requirements of hysteretical systems. Essentially two equivalent models are useful for such analysis. The first is based on the magnetization of a set of ferromagnetic monodomains. This is the above mentioned Preisach model. We use it to predict the optical hysteresis. The second describes the magnetization of bulk ferromagnets in terms of irregular displacement of Bloch walls. We also utilize an analogous scheme to this second model introduced by Sixtus and Tonks [16] in their analysis of the magnetization processes under mechanical stresses. This allows us to very simply describe the optical hysteresis and the shape of the resulting loop with two competing characteristic beam powers. These two powers represent, respectively, the threshold of laser-induced phase transition and the threshold of optical droplet trapping, similar in many respects to the so-called nucleation and propagation magnetic fields. Besides, we also focus our attention on much more complicated behaviors of hysteretical systems, generally not very well studied: the existence of a limit hysteresis loop of a cyclically excited medium [17] and the cycle creep phenomenon, also known as "reptation" after Néel original work [18]. These intrinsic properties, often disregarded in the fundamental studies but which have important practical consequences, also deserve to be analyzed. We observe that, as in ferromagnets, successive hysteresis loops of the cyclically excited liquid mixture are not exactly reproducible and stabilize after a few runs. A striking result is also the observation of the cycle creep. When the medium is cycled from the upper part of the hysteresis loop, the system exhibits a slow positive drift towards a laser beam self-focusing of increasing quality.

The paper is organized as follows. We present in Sec. II the fundamental processes of the first-order phase transition generated by the laser wave. In Sec. III we experimentally describe the expected phase separation induced in a micellar phase of microemulsion and we characterize its morphology and its optical properties. In Sec. IV we present the experimental analysis of the hysteretical laser beam self-focusing generated by the induced phase transition. We interpret the results quantitatively and discuss them with respect to an analogy with the magnetization processes in bulk ferromagnets. We finally conclude in Sec. V by giving some prospects of the present study.

II. PHASE SEPARATION INDUCED BY A cw LASER WAVE

The state of the binary liquid studied will be thermodynamically described by the temperature T, the concentration (i.e., mass fraction) C of one of the components, and the hydrostatic pressure P. In the following, we consider a one-phase mixture located in the vicinity of the liquid-liquid coexistence curve in the phase diagram. It is submitted to a low power cw laser beam radiation. Therefore global density variations due to the hydrostatic compression of both species can be neglected in comparison with those due to the osmotic compressibility of the mixture. The hydrostatic pressure is then supposed to be constant.

Let C_0, T_0, be the values of C, T in the absence of the electromagnetic field, and C_E, T_E be their field-induced variations:

$$C=C_0+C_E\ ,\quad T=T_0+T_E\ . \tag{1}$$

T_E and C_E can be evaluated at the first order with respect to the optical intensity $|E|^2$ by solving the field-modified mass and thermal diffusion equations [19]. Notice that if we analyze the field interaction during time scales very large compared to the thermal and density characteristic times of diffusion, these equations reduce to their stationary limits. Assuming cylindrical symmetry, one finds at a distance r from the z axis of propagation [19]

$$T_E(r,z)=B_1P(z)U\left[\frac{r^2}{a^2(z)}\right]\ , \tag{2a}$$

$$C_E(r,z)=B_2K_T|E(r,z)|^2-B_1\frac{k_T}{T_0}P(z)U\left[\frac{r^2}{a^2(z)}\right]\ , \tag{2b}$$

where the wave interacting with the medium is supposed

to be a Gaussian cw laser beam of intensity (TEM_{00} mode)

$$|E(r,z)|^2=\frac{8}{c_1\sqrt{\varepsilon_L}}\frac{P(z)}{a^2(z)}e^{-r^2/a^2(z)} . \quad (3)$$

$P(z)$ is the incident beam power and $a(z)$ the beam radius. $k_T=-T_0\nabla C/\nabla T$ is the thermodiffusive ratio and $K_T=(1/C_0)(\partial\Pi/\partial C)_0$ is the osmotic compressibility which characterizes the electrostrictive process. The B_1 and B_2 constants are defined by $B_1=\alpha_a/\pi\Lambda$ and $B_2=(C_0^2/8\pi)(\partial\varepsilon_L/\partial C)_0$ where ε_L corresponds to the linear part of the dielectric constant ε of the medium (i.e., $\varepsilon=\varepsilon_L+\varepsilon_E$), α_a is the absorption coefficient at the used wavelength, Λ the thermal conductivity, and c_1 the light velocity in vacuum. The function U depends on the boundary conditions of the problem. If one supposes $T_E=0$ at some very large transverse distance $r=a_{cl}$ compared to the beam radius $a(z)$, U can be expressed as [20]

$$U\left[\frac{r^2}{a^2(z)}\right]\cong 0.25\left[\ln\left[\gamma\frac{a_{cl}^2}{a^2(z)}\right]-\frac{r^2}{a^2(z)}\right] , \quad (4)$$

where $\gamma=1.781$. This concentration variation leads to the following local variation of the osmotic pressure:

$$\Pi_E\cong\left[\frac{\partial\Pi}{\partial C}\right]_0 C_E=\frac{1}{K_T C_0}C_E .$$

To describe the fundamental processes, we assume an off-resonance wave-medium coupling. Then, the intrinsic temperature increase T_E has a negligible influence on the thermodynamical path followed in the phase diagram compared to the concentration shift C_E. In the case of mixtures characterized by a strong thermodiffusive effect [12], this approximation is reasonable and allows us to consider the wave-medium coupling as isothermal. The mixture evolution in the presence of the field will then be depicted by an isothermal path in the phase diagram. In the experimental section, the bindary liquid analyzed is characterized by a negative value of C_E because k_T is positive. Then, in order to induce a phase separation with the field, we choose a one-phase sample of initial concentration C_0 located in the vicinity of the liquid-liquid coexistence curve on the high concentration side of the phase diagram as illustrated in Fig. 1 in the (C,Π) plane. The increase in the incident laser beam power induces an isothermal decrease in the concentration, resulting in a beam-centered optical quenching of the mixture in the metastable region as soon as $|C_E|>|C_1'-C_0|$. Owing to fluctuations, this quenching into the two-phase region results in a local phase separation through the nucleation of droplets constituted of droplets constituted by the minority phase of concentration C_2 [21].

III. EXPERIMENTAL ANALYSIS OF THE INDUCED PHASE SEPARATION

A. Experimental setup and characteristics of the chosen mixture

A schematic of our experimental setup is presented in Fig. 2. The liquid mixture is contained in an optical fused quartz cell thermally controlled and located at the focal point of a $\times 10$ microscope objective L_1 which focuses a cw Ar^+ laser beam (wavelength $\lambda_0=5145$ Å in vacuum) on the entrance face of the cell ($z=0$). The evolution of the interaction inside the laser beam is visualized and recorded transversally to the beam axis, by means of an optical system composed of a $\times 20$ microscope objective and a charge-coupled device (CCD) video camera coupled to a VCR and a personal computer. This system also allows us to localize the beam waist a_0 inside the cell. Values of a_0 ranging from 2 to 20 μm can be achieved by varying the optical path between the two lenses L_1 and L_2 ($f_2=200$ mm). The lens L_3 ($f_3=32$ mm) images the output face of the cell on the circular di-

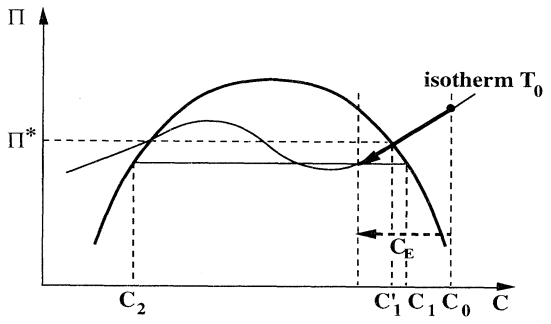

FIG. 1. Schematic phase digram of a binary liquid mixture. C is the concentration of one of the components and Π is the osmotic pressure. Π^* illustrates the Maxwell plateau value at temperature T_0. C_E denotes the isothermal optical quench in composition in the metastable region from C_0, C_1' is the concentration at the intersection between the coexistence curve and the path followed by the optical quench, C_1 and C_2 are the coexisting concentrations associated with the quench C_E.

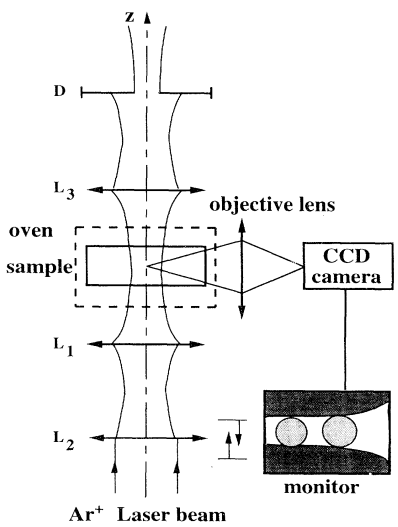

FIG. 2. Experimental setup.

aphragm D. The transmission of D can be considered as a measure of the beam radius at the output of the medium. It is used to quantitatively analyze the hysteretic behavior of the system beam medium as discussed in the next part of the paper.

To experimentally investigate the phase separation induced by concentration variations generated by the wave, we choose miscellar phases of microemulsions as test media because they have a large sensitivity to laser waves. Owing to the supramolecular size of the micelles, both electrostrictive and thermodiffusive processes can lead to measurable micellar concentration variations on the beam axis (in our case a decrease in the micellar concentration) and thus are able to induce a phase separation. Moreover, since the intrinsic absorption of those mixtures at the wavelength used is weak and k_T is large, such a phase transition can be considered, as a first approximation, as isothermal, particularly in the vicinity of a critical point.

A microemulsion is a quaternary component mixture of water, oil, surfactant (soap), and cosurfactant (alcohol) which is characterized by a very large structural diversity. The selected system has the following mass composition: water 5%, *n*-dodecane 78%, sodium dodecyl sulfate 4.8%, and 1-pentanol 12.2%. Its phase diagram has been reported elsewhere [22]. Located in the rich-oil part of this diagram, it features a micellar phase at room temperature which corresponds to a stable suspension of very small spherical water droplets of approximately 4 nm in diameter isolated from the oil (i.e., *n*-dodecane) by a shell of amphiphilic molecules (i.e., surfactant) adsorbed at the water-oil interface. These particles, called inverted micelles, can be considered from the optical point of view as a set of dielectric spheres suspended in a continuous oil phase of varying dielectric constant. The composition of our particular micellar phase was chosen close to a coexistence curve between a high critical temperature $T_C = 31\,^{\circ}\mathrm{C}$ and a low off-critical temperature of phase separation $T_D = 20\,^{\circ}\mathrm{C}$ so that a very small decrease of the micellar concentration induces a phase separation of liquid-liquid type towards a micellar phase of lower concentration.

In this particular system, we have shown that the electrostrictive variation in concentration is negligible [14]. The interaction between the wave and the micellar phase is mainly controlled by the thermodiffusive process, which results in a local decrease of the micellar concentration inside the beam. In the case illustrated in Fig. 1, this thermodiffusive coupling generates a phase separation between the micellar phase of concentration C_1 and the associated minority phase of lower concentration C_2. A very small concentration decrease $(C_1' - C_0)$ evaluated to be $\approx 44 \times 10^{-3}$ in the beam center at $T_0 = 298$ K is required to induce this phase separation. In the vicinity of the critical point, strong values of the thermodiffusive constant k_T (i.e., $k_T = k_T^0 [(T_c - T_0)/T_c]^{-\nu}$ with $k_T^0 \approx 4$ and $\nu = 0.63$) have been measured. So low cw laser powers are able to induce a sizable concentration variation. At this temperature, an incident laser beam power of the order of 100 mW is sufficient to induce the transition [14].

B. Morphology of the induced phase separation

When the medium is submitted to a laser power higher than this threshold power, the resulting morphology is strongly dominated by the difference of optical properties between the two coexisting phases. The contrast of micellar concentration between C_1 and C_2 leads to a contrast in dielectric constant $\Delta\varepsilon = \varepsilon_2 - \varepsilon_1 \approx (\partial\varepsilon_L/\partial C)_0 (C_2 - C_1)$. Since $(\partial\varepsilon_L/\partial C)_0 = -5.69 \times 10^{-2}$ and $(C_2 - C_1)$ are both negative in our particular case, the index of refraction of the low concentration phase is larger than that of the surrounding phase. From the phase diagram [22], one has $\Delta C = (C_2 - C_1) = \Delta C_0 [(T_c - T_0)/T_c]^{\beta}$ and $\Delta\varepsilon_L = (\Delta\varepsilon_L)_0 [(T_c - T_0)/T_c]^{\beta}$ with $\beta = 0.32$, $\Delta C_0 = -1.91$, and $(\Delta\varepsilon_L)_0 = 0.109$. One could expect the generation of a beam-centered cylinder of the new phase of concentration C_2 in the majority phase of concentration C_1. However, such a cylinder cannot exist at steady state if the wetting properties of the liquid on the walls of the cell do not have a preeminent influence on the dynamics of the separation. This is the case when the optical path 1 of the beam in the cell is much larger than the laser beam circumference: $1 \gg 2\pi a$ [23]. The hydrodynamic instability of the cylinder results from interface fluctuations (Rayleigh-like instability). Corrugations develop in its envelope which ultimately lead to a cylinder breaking into discrete droplets [24] because the wetting processes on the cell edges are not sufficiently strong to preserve this structure. This was clearly observed in our experimental conditions as illustrated in Fig. 3. The mixture is contained in a fused quartz cell (2 mm thick and 1 cm wide). A laser beam of power $P_i = 0.24$ W and beam waist $a_0 = a(z = 0) = 12\ \mu$m propagates inside the sample at room temperature $T_0 = 298$ K. Under these conditions, the optical quenching conditions are fulfilled and the phase separation occurs. A droplet is generated by heterogeneous nucleation on the entrance face of the cell containing the sample [Fig. 3(a)]. The very slow dynamics of the early growth stage of the droplet [Figs. 3(a) and 3(b)] is controlled by mass diffusion [14]. Typically, 10 min are

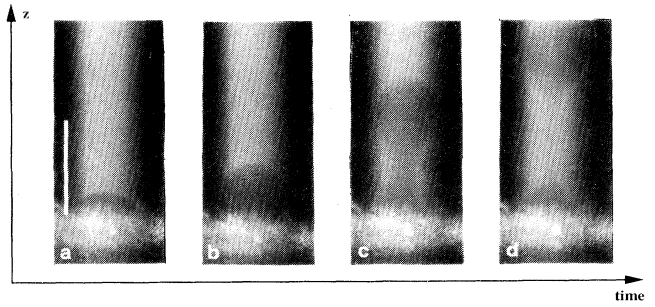

FIG. 3. Growth [(a), (b)] and hydrodynamic destabilization [(c), (d)] of a droplet nucleated heterogeneously at the internal entrance face of the cell containing the sample, when the optical path is large compared to the beam waist. z is the laser beam propagation axis. The control parameters are $1 = 2$ mm, $a_0 = 12\ \mu$m, $P_i = 240$ mW, $T_0 = 298$ K. The bar corresponds to 100 μm.

spent on this stage before the destabilization of the cylinder [Fig. 3(c) and 3(d)] which is, in comparison, very fast (≈ 1 s).

As a consequence, when $1 \gg 2\pi a$ droplets are continuously nucleated owing to the continuous field action on the medium. Since the droplet polarizability p_d is proportional to its volume, the electrostrictive energy $W=-1/2p_d|E|^2$ is in fact much larger than the Boltzmann energy $k_B T_0$. Typically, at room temperature one obtains $|W|/k_B T_0 \approx 3\times 10^3$ for a droplet radius $r_d \approx a_0 = 5$ μm and an incident beam power $P_i = 0.1$ W. One then expects the generation of a set of droplets trapped on the beam axis. This optical trapping is illustrated in Fig. 4, which also shows that the droplets self-trap the laser beam. Each generated droplet acts as a spherical lens (i.e., ball lens). Thus the medium behaves as a set of self-induced ball lenses which focus the laser beam. This self-focusing process is quite original since it is not generated by optical nonlinearities [19], which are negligible in our particular system, but corresponds instead to a linear propagation in a self-induced unhomogeneous liquid manipulated and arranged by the field itself.

It is also important to consider the case $1 \leq 2\pi a$ where the phase separation is completely dominated by the wetting properties of the two phases [25]. The corresponding behavior of the phase separation has been experimentally observed using a capillary quartz cell ($1=100$ μm) to contain the mixture. If the minority phase is more wettable to fused quartz than the phase of concentration C_1, as in our mixture, the droplets gradually wet the inner cell edges and form wetting layers localized over a surface of the order of the beam section. Since these layers cannot develop too far outside the beam, they necessarily grow inside the illuminated volume and eventually collide. This coalescence gives birth to a beam-centered domain of the minority phase which fills up the cell containing the sample between its edges across the beam section. Neglecting the small axial curvature of this domain, it can be approximated by a cylindrical column of section πa^2 and length 1. Since the refractive index of this cylinder is larger than that of the surrounding phase, the beam propagation inside the medium is strongly modified. The self-focusing condition [26] is satisfied in our conditions and, as a result, the beam creates for itself its own waveguide. It can be noticed from Figs. 3(c) and 3(d) that the neck induced during the Rayleigh-like instability generates a completely equivalent self-guiding of the wave. This self-trapping is observed through the bright filament appearing at the exit of the neck in the droplet being expelled.

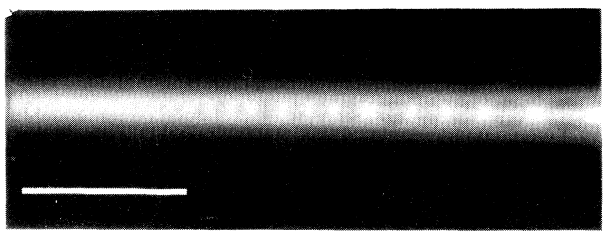

FIG. 4. Optical trapping of the droplets induced by the optical quench, and related laser beam self-focusing (essentially observed on the right part of the photograph). The left part corresponds to the entrance face of the cell. The control parameters are $1=2$ mm, $a_0=6$ μm, $P_i=220$ mW, $T_0=298$ K. The bar corresponds to 100 μm.

IV. HYSTERESIS OF THE LASER BEAM SELF-FOCUSING

A. Optical bistability and optical hysteresis

In the previous case, $1 \leq 2\pi a$, the strong self-focusing of the beam in the cylinder and the S-shaped structure of the isotherms associated to the induced first-order phase transition together lead to an intrinsic optical bistability. This bistable behavior can be described in a general way if one considers the equation of state of the mixture. Not too far from the critical point, this equation reduces to a universal form. In the mean-field approximation it reads [27]

$$\mathcal{P} = A_1 + A_2 \tau \Phi + A_3 \Phi^3 , \tag{5}$$

where A_1, A_2, and A_3 are positive constants depending on the chosen microscopic model which describes the interactions taken into account. $\mathcal{P}$, τ, and Φ are the osmotic pressure, the temperature, and the volume fraction of micelles normalized to their critical values Π_C, T_C, and ϕ_C:

$$\mathcal{P} = \left[\frac{\Pi-\Pi_C}{\Pi_C}\right] , \quad \tau = \left[\frac{T-T_C}{T_C}\right] , \quad \Phi = \left[\frac{\phi-\phi_C}{\phi_C}\right] . \tag{6}$$

When $\tau<0$ (i.e., two-phase region in the phase diagram), in a certain range of $\mathcal{P}$ the function $\Phi(\mathcal{P},\tau)$ defined by Eq. (5) becomes three-valued. Since the dielectric constant depends on the thermodynamical state of the medium [i.e., $\varepsilon_L = \varepsilon_L(\mathcal{P},\tau,\Phi)$], this nonuniqueness of the state of the mixture may lead to a multivalued variation of ε_L with respect to $\mathcal{P}$. A simple linear approximation of the Clausius-Mossotti relation allows us to express it as a function of the order parameter Φ of the phase transition during the phase separation:

$$\varepsilon_L \approx (\varepsilon_L)_0 + \left[\frac{\partial \varepsilon_L}{\partial \Phi}\right]_0 \Phi . \tag{7}$$

The substitution of Eq. (7) in Eq. (5) gives the variation of the ε_L as a function of $\mathcal{P}$ at the fixed reduced temperature τ. This function is illustrated in Fig. 5 for $(\partial\varepsilon_L/\partial\Phi)_0<0$ in the case where it features an S-shaped variation (i.e., $\tau<0$). $\mathcal{P}^*$ is the Maxwell plateau value. In the metastable region $[\mathcal{P}^*-\delta\mathcal{P}_m, \mathcal{P}^*+\delta\mathcal{P}_m]\varepsilon_L$ is, as expected, multivalued, the intermediate value being unstable. If one assumes that a metastable state can last as long as the mixture is kept in the multivalued range of the control parameter $\mathcal{P}$, an intrinsic bistable propagation takes place when an initial one-phase sample (i.e., $\mathcal{P}_0 > \mathcal{P}^* + \delta\mathcal{P}_m$) is

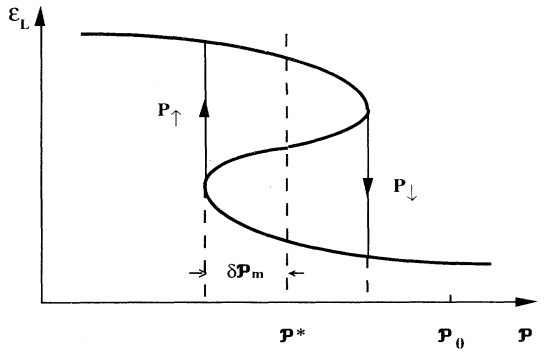

FIG. 5. Schematic representation of the variation in the dielectric constant ε_L with the osmotic pressure $\mathcal{P}$ during a first-order phase transition when $(\partial\varepsilon_L/\partial C)_0<0$ and $T_0<T_C$ (as in our experimental case). A beam power increase leads to a decreasing variation in $\mathcal{P}$ from its initial value $\mathcal{P}_0$, chosen outside the coexistence curve. When the beam power $P_\uparrow$ is reached ε_L switches from the lower to the upper part of its S-shaped variation. When the beam power is lowered from the upper part, the switching occurs at $P_\downarrow$.

chosen because $\mathcal{P}_E=(\Pi_E-\Pi_C)/\Pi_C<0$. The switching up and down occur, respectively, at the beam power thresholds $P^\uparrow$ and $P_\downarrow$ defined by $\mathcal{P}_E(P^\uparrow)=\mathcal{P}^*-\delta\mathcal{P}_m-\mathcal{P}_0$ and $\mathcal{P}_E(P_\downarrow)=\mathcal{P}^*+\delta\mathcal{P}_m-\mathcal{P}_0$. The resulting bistable wave guiding could in principle be analyzed with the experimental setup described in Fig. 2, by measuring the power P_t transmitted by the diaphragm D as a function of the incident power P_i. However, owing to the slight thickness of the sample, such a basic behavior of one domain is difficult to observe.

Equivalently, if one now considers the case $1\gg 2\pi a$, where a set of droplets is generated and trapped on the laser beam axis, each droplet in its surrounding medium behaves as a bistable propagation element. Moreover, the associated lensing effect modifies the field distribution and induces optical couplings between droplets. In other words, the optical response of the medium corresponds to a propagation in a set of self-induced coupled bistable elements. Therefore, in the case $1\gg 2\pi a$, optical hysteresis is expected in the propagation of the field. This optical response can be better understood with the use of a ferromagnetic analogy. Except when the magnetic field is orthogonal to the minimum energy direction, the magnetization curve of a small isolated ferromagnetic monodomain features a rectangular loop with two stable states "up" and "down" (bistable behavior) [6]. Moreover, in a bulk ferromagnet, the irreversible couplings, in the thermodynamical sense, between a large number of domains result generally in a "classical" smooth hysteresis loop. Since the bulk can be schematically represented by a set of interacting grains (domains) oriented at random [28], one an therefore say that hysteresis corresponds to the overall behavior of coupled elements which are characterized by a bistable loop [15]. However, it can be objected that the magnetization of a ferromagnet does not result from a phase transition, but corresponds instead to a manipulation of the domain structure by the magnetic field. Thus the previous magnetic analogy would be debatable. In fact, strictly speaking, the magnetic analogy has to be developed with the magnetization of a metamagnetic material which involves an antiferromagnetic-ferromagnetic transition when the medium is submitted to an increasing magnetic field [29]. In this case, the magnetization starts varying linearly with the magnetic field (antiferromagnetic phase), until the field becomes strong enough to tilt the spins of the antiferromagnet structure. Ferromagnetic domains are then nucleated, grow, and their magnetic field manipulation leads to a hysteretical response to the medium. Therefore, since we are interested in the properties of the more ordered phase (here the ferromagnetic one) as well as in the associated hysteresis loop, a ferromagnetic analogy can be directly developed without any ambiguity.

B. Experimental evidence of hysteretical behavior

The laser beam self-focusing is quantitatively analyzed by recording the power P_t transmitted through the diaphragm D while increasing the incoming power P_i, as illustrated in Fig. 2. Figure 6 gives an experimental variation of P_t as a function of P_i for a beam waist $a_0=2.2$ μm at the temperature $T_0=24.5$ °C, when the aperture of D is chosen so as to transmit one-half of the incident power. The systematic error on each measured beam power is ± 5 mW. The lower dashed line illustrates the variation in P_t when the medium has a linear behavior ($P_t=0.5P_i$). The higher dashed line represents the variation if the diaphragm D is completely opened ($P_t=P_i$). The experimental points shown by open circles and

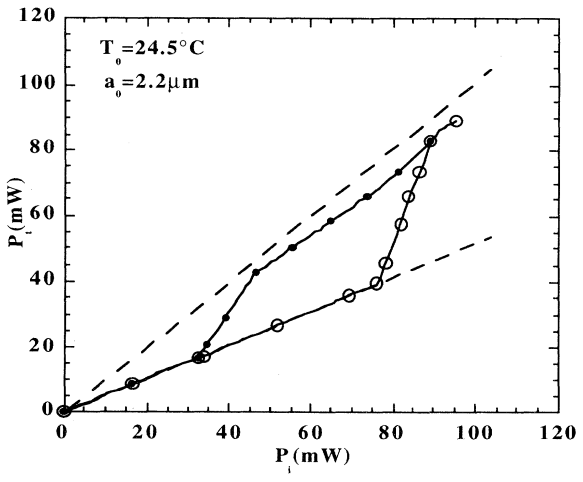

FIG. 6. Experimental variations in the transmitted power P_t as a function of the incident power P_i for $T_0=24.5$ °C and $a_0=2.2$ μm. The experimental points describe the increasing (○) and the decreasing (●) variations in P_t at optical steady state, and illustrate the expected hysteretical self-focusing. The lower (higher) dashed line represents the variations in P_t when the diaphragm transmission is one-half (one).

closed circles describe, respectively, the increasing and the decreasing variations of the transmitted power P_t. It is important to note that each point corresponds to a steady state for the beam propagation in the medium. Practically, the measurement is done a few minutes after the increase in the incident beam power. This time is large compared to the characteristic time scale of micelle diffusion. It appears in Fig. 6 that as long as the incident power is smaller than a threshold power called $P_\uparrow$, the transmission equals one-half. Thus, as already mentioned, the optical nonlinearity of the initial phase, if it exists, is extremely small and is not detectable. Our micellar system can be considered as optically linear. When $P_i \geq P_\uparrow$ the curve suddenly deviates from the one-half transmission to a transmission approximately equal to one. When the incident power is decreased, this latter transmission is preserved until a second threshold $P_\downarrow$ below which the beam propagation recovers its linearity. A typical example of beam propagation and transverse beam profile before and during the self-focusing process is given in Fig. 7. The propagation at low beam power without self-focusing is illustrated in Figs. 7(a) and 7(b). The self-focusing appears as a bright filament resulting from the propagation in a self-induced set of ball lenses [Fig. 7(c)] corresponding to the simultaneous increase in intensity in the central part of the beam spot [Fig. 7(d)].

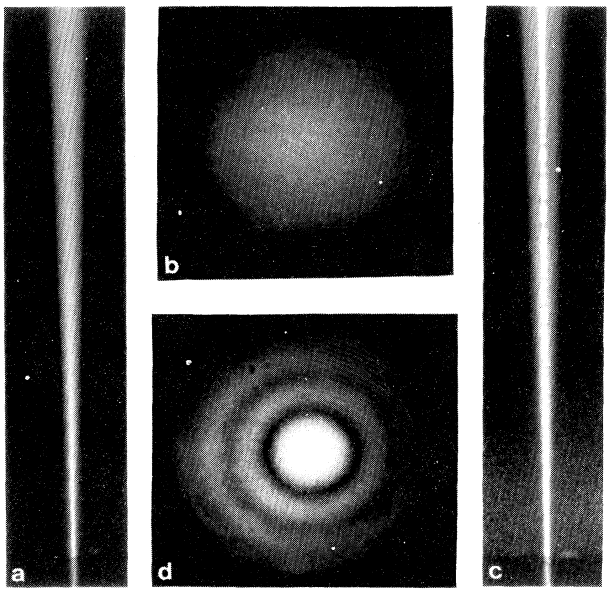

FIG. 7. Beam propagation and transverse beam profile below [(a), (b)] and above [(c), (d)] the self-focusing threshold $P_\uparrow$, at room temperature for $a_0=2.5$ μm. These photographs illustrate the beam propagation over one of the 2 mm of the cell length. (b) and (d) represent images of the transverse beam profile at the exit face of the cell. (a) and (b) show a classical linear propagation. (c) illustrates the laser beam self-focusing induced by the beam-trapped droplets generated by the optical quench in composition. The corresponding transverse beam profile (d) shows the intense beam spot resulting from this strong self-focusing process.

C. Temperature evolution of threshold powers

The strong laser beam self-focusing involves the nucleation of droplets and thus the dynamics of the induced phase separation after the optical quench. To optically nucleate droplets, the incident beam power P_i has to reach a phase transition threshold $(P_\uparrow)_{PT}$ necessary to cross the coexistence curve and to overcome the effect of the activation barrier which prevents any noticeable nucleation process. If $(C_E)_C$ denotes the smallest field-induced variation of concentration above which nucleation starts, this characteristic input beam power is given by

$$(P_\uparrow)_{PT}=\frac{-(C_E)_c}{B_1}\frac{T_0}{0.25\ln(\gamma a_{cl}^2/a_0^2)}\frac{1}{k_T} . \tag{8}$$

However, the self-focusing process also involves the trapping on the beam axis of the nucleated droplets whose ball-lens behavior is responsible for the propagation disturbance. The trapping force has to overcome the Brownian motion. This condition will be satisfied when the electrostrictive coupling W satisfies the relation $|W|=1/2p_d|E|^2>k_BT_0$. The smallest input beam power needed to verify this inequality leads to an optical trapping threshold $(P_\uparrow)_{rad}$, given in mks units by

$$(P_\uparrow)_{rad}=k_BT_0\frac{c_1\sqrt{\varepsilon_L}\pi a_0^2}{p_d} , \tag{9}$$

with

$$p_d=4\pi\varepsilon_1\left[\frac{\varepsilon_2-\varepsilon_1}{\varepsilon_2+2\varepsilon_1}\right]r^3 . \tag{10}$$

The particle radius r has to be specified at the threshold $(P_\uparrow)_{rad}$ since its value evolves during the phase transition. This droplet growth has been analyzed elsewhere [14]. In fact, the droplet radius which has to be taken into account in Eq. (9) must be of the order of the critical radius r_c. Indeed, the presence of a droplet inside the beam and its subsequent growth implicitly suggest that it has been trapped since its "birth." An order of magnitude of the critical radius r_c can then be estimated as follows. Since the optical quench in composition involves micelle diffusion, the characteristic time necessary to induce a critical droplet is related to the mass diffusion of a micelle over a distance of the order of the beam radius. It results in [30]

$$r\approx r_c\approx(a_0^2r_{mic})^{1/3} , \tag{11}$$

where r_{mic} is the radius of a micelle. From Eq. (9), it is then seen that $(P_\uparrow)_{rad}$ is essentially dependent on the dielectric constant contrast $\Delta\varepsilon=\varepsilon_2-\varepsilon_1$:

$$(P_\uparrow)_{rad}=\frac{3k_BT_0c_1\sqrt{\varepsilon_L}}{\Delta\varepsilon r_{mic}} , \tag{12}$$

where we have approximated $\varepsilon_2+2\varepsilon_1$ by $3\varepsilon_1$.

Since both conditions $P>(P_\uparrow)_{PT}$ and $P>(P_\uparrow)_{rad}$ have to be simultaneously satisfied in order to self-focus the beam, the experimental value of $P_\uparrow$ is determined by the

largest of these two threshold powers. To identify the process which drives the experimental behavior, it is important to analyze the behavior of both thresholds when approaching the critical temperature T_C. From Eqs. (8) and (12), it can be noticed that these critical behavior are respectively dominated by the variations in k_T and Δ_ε.

As a consequence, when varying T_0, the following behaviors are expected. Far from the critical point, the refractive index contrast is large, leading to a phase transition threshold $(P_\uparrow)_{PT}$ larger than $(P_\uparrow)_{rad}$. The laser beam self-focusing is entirely controlled by the induced phase separation process. As soon as a droplet is nucleated, it is automatically trapped in the beam center. Moreover, according to the critical behavior of k_T, $P_\uparrow$ [i.e., $(P_\uparrow)_{PT}$ in this regime] decreases when T_0 increases and approaches T_C. Otherwise, in the vicinity of the critical point, the refractive index contrast between the droplets and their surrounding phase vanishes, whereas k_T becomes large. In this case, the behavior of the laser beam self-focusing is governed by the droplet trapping and then by the variations in $(P_\uparrow)_{rad}$ with T_C-T_0. $P_\uparrow$ diverges with the exponent β characterizing the behavior of $\Delta\varepsilon$.

The experimental temperature evolution of $P_\uparrow$ is reported in Fig. 11. As expected, $P_\uparrow$ diverges when approaching the critical point according to a simple power law. The measured critical exponent 0.28 is near the theoretical value $\beta=0.32$. More precisely the fit of the experimental variation in $P_\uparrow$ when $T_C-T_0<4$ K leads to the following equation: $P_\uparrow=0.140(T_c-T_0)^{-0.28}$ whereas Eq. (12) leads to the theoretical variation $(P_\uparrow)_{rad}=0.153(T_c-T_0)^{-0.32}$ without any adjustable parameter. This good agreement between experimental and theoretical laws confirms that the droplet trapping is the dominant process near the critical point. Furthermore, Fig. 8 shows that $P_\uparrow$ decreases when T_0 increases in the domain $T_C-T_0>5$ K. As expected, the droplet nucleation is the dominant process in this domain and $P_\uparrow$ follows the variations in $(P_\uparrow)_{PT}$. However, this temperature range is too far from the critical point and the number of accessible experimental points of this part of the curve is to low to lead to a measure of the critical exponent ν characteristic of the thermodiffusive constant k_T. It is possible only to quantitatively extract from Fig. 8 the experimental value of the crossover between both regimes, the one dominated by $(P_\uparrow)_{rad}$, and the other by $(P_\uparrow)_{PT}$. One finds $(T_C-T_0)\approx 4.5$ K. This crossover is theoretically obtained by equating $(P_\uparrow)_{rad}$ and $(P_\uparrow)_{PT}$. A numerical application from Eqs. (8) and (12) leads to a theoretical value $(T_C-T_0)=5$ K, in good agreement with experimental results.

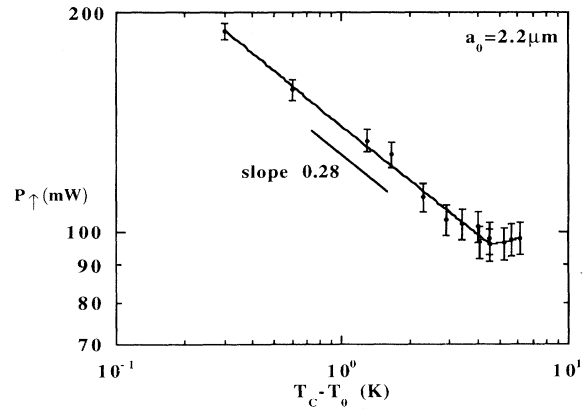

FIG. 8. Temperature evolution of $P_\uparrow$ for $a_0=2.2$ μm illustrating two different behaviors. Near T_C, $P_\uparrow$ reflects the droplet-trapping threshold $(P_\uparrow)_{rad}$ which diverges with the critical exponent β.

D. Analogy between optical and ferromagnetic hysteresis

The preceding section briefly indicated how the magnetization of a set of coupled ferromagnetic grains makes it possible to predict the observed hysteretical behavior of the beam propagation in an optically quenched medium. This analogy can also be directly discussed from the properties of a bulk ferromagnet composed of a large number of domains separated by walls. In these materials, the magnetization processes are strongly dependent on the wall displacements. A phenomenological description has been given in terms of the so-called nucleation and propagation magnetic fields H_N and H_P [16]. If we consider a bulk ferromagnet magnetized at saturation in one direction, there is only one domain. To switch the magnetization, one has to nucleate a domain in the opposite direction and to induce its growth throughout the sample. The generation of this nucleus needs an externally applied magnetic field $H\geq H_N$. Moreover, its growth is possible only if $H\geq H_P$. The shape of the resulting hysteresis loop depends on the ratio H_N/H_P. If one assimilates $(P_\uparrow)_{PT}$ to H_N and $(P_\uparrow)_{rad}$ to H_P an equivalent scenario is observed in our experiments.

1. Case $(P_\uparrow)_{PT} \gg (P_\uparrow)_{rad}$

If $H_N \gg H_P$ in a bulk ferromagnet, a square hysteresis loop with abrupt variations in regimes is expected. As soon as H_N is reached, nuclei are generated and instantaneously fill the whole sample. Similarly, as soon as $(P_\uparrow)_{PT}$ is reached, a first droplet of index $n_1=n_0+\Delta n$ is

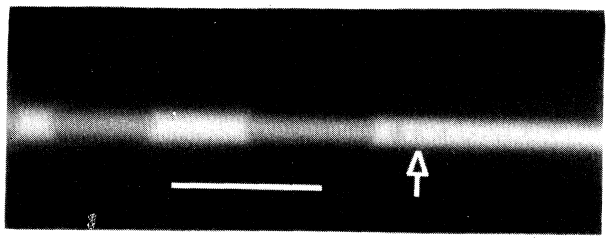

FIG. 9. Instability mechanism during the self-focusing process. A set of very small droplets (shown by the arrow) is induced at the intermediate beam waist resulting from the ball-lens behavior of the nearest beam-trapped droplet. The control parameters are $l=2$ mm, $a_0=6$ μm, $P_i=220$ mW, $T_0=298$ K. The bar corresponds to 50 μm.

nucleated in the medium of index n_0 at the beam waist and automatically trapped. It grows inside the beam, and around the new beam waist generated by its associated lens effect the conditions of homogeneous nucleation are satisfied again. A new droplet is thus nucleated. It grows, focuses light, induces another beam waist, and so on. This instability mechanism can be analyzed in the paraxial ray approximation, using the *ABCD* matrix formalism to describe the beam propagation [31]. Assuming a beam waist a_0 located at the entrance of the first ball lens, we can determine the dimension a_1 and the position d_1 of the new waist induced by this lens [30]:

$$a_1^2 = a_0^2 \frac{1}{\left[1-2\frac{\Delta n}{n_1}\right]^2 + \left[\frac{2\pi n_0 a_0^2}{\lambda_0 r}\right]^2 \left[2\frac{\Delta n}{n_1}\right]^2}, \tag{13}$$

$$\frac{d_1}{r} = \frac{\left[\frac{2\pi n_0 a_0^2}{\lambda_0 r}\right]^2 \left[2\frac{\Delta n}{n_1}\right]\left[1-2\frac{\Delta n}{n_1}\right] - 2\left[1-\frac{\Delta n}{n_1}\right]\left[1-2\frac{\Delta n}{n_1}\right]}{\left[1-2\frac{\Delta n}{n_1}\right]^2 + \left[\frac{2\pi n_0 a_0^2}{\lambda_0 r}\right]^2 \left[2\frac{\Delta n}{n_1}\right]^2}. \tag{14}$$

Since the droplet growth is limited by the transverse intensity distribution, we assume $r = a_0$ for the first generated droplet at optical steady state. At $(T_C - T_0) = 6$ K one finds a focal length $d_1 = 35$ μm and a ratio $a_1/a_0 = 0.86$ (we have chosen $a_0 = 2.2$ μm). Thus, if in a_0 at first droplet has been nucleated, then the above value of a_1 shows that the conditions of nucleation are again satisfied beyond this droplet and particularly in d_1. New droplets are then nucleated step by step. This behavior is illustrated in Fig. 9. At an intermediate beam waist, a homogeneous nucleation process leads to the generation of a set of very small droplets (indicated by an arrow) which eventually collide, giving rise to a large one. As a consequence, when $P_i \geq (P_\uparrow)_{PT}$ droplets completely fill the volume crossed by the wave and induce the strong laser beam self-focusing illustrated in Fig. 10 (case $T_C - T_0 = 6$ K) by the slope breaking in $P_\uparrow$. This instability mechanism can also be directly observed from a stability analysis of the ascending part of the hysteresis loop. If just beyond $P_\uparrow$ the incident power is slightly decreased before a complete stabilization of the transmitted power, the strong self-focusing first initiated in $P_\uparrow$ is not affected.

Moreover, after a complete stabilization of the self-focusing, if the incident beam power is decreased, the beam-trapped droplets remain thermodynamically stable as long as the condition $|C_E| > C_0 - C_1'$ is preserved. Finally, because of the strong wave focusing generated by the set of droplets, the conditions for nucleation also remain satisfied, particularly at the induced intermediate beam waists [$(P_\uparrow)_{PT}$ is a slightly increasing function of a_0]. This irreversible nucleation represents the main process at the origin of the hysteretical behavior illustrated in Fig. 10.

2. Case $(P_\uparrow)_{rad} \gg (P_\uparrow)_{PT}$

In a bulk ferromagnet, a square hysteresis loop is also expected in the case $H_P \gg H_N$. Indeed, even if nuclei are induced when the magnetic field reaches H_N, they cannot develop because $H < H_P$. They are "frozen" and eventually decrease in size and disappear. However, as soon as $H > H_P$, the generated nuclei are able to grow and thus

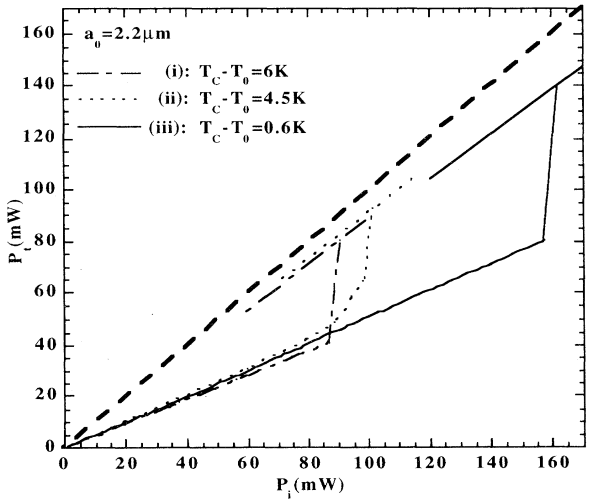

FIG. 10. Hysteretical behavior as a function of the ratio between the phase transition and the droplet-trapping thresholds: (i) $(P_\uparrow)_{PT} \gg (P_\uparrow)_{rad}$ (case $T_C - T_0 = 6$ K), (ii) $(P_\uparrow)_{PT} \approx (P_\uparrow)_{rad}$ (case $T_C - T_0 = 4.5$ K), and (iii) $(P_\uparrow)_{PT} \ll (P_\uparrow)_{rad}$ (case $T_C - T_0 = 0.6$ K). The higher dashed line represents the variations in P_t when the diaphragm transmission equals one.

invade the bulk. This behavior is again completely analogous to that of the optical hysteresis in the case $(P_\uparrow)_{rad} \gg (P_\uparrow)_{PT}$ for which the self-focusing is controlled by the droplet trapping inside the beam. When the condition $P_i \geq (P_\uparrow)_{PT}$ is reached, critical droplets are nucleated at the beam waist, but the electrostrictive forces are too small to trap them efficiently. They diffusive outside the beam and disappear. The wave propagation remains linear. One has to increase the incident beam power until $P_i \geq (P_\uparrow)_{rad}$. From this threshold, nuclei are trapped in the wave. They grow inside the beam, behave as ball lenses, and the instability mechanism described above in the case $(P_\uparrow)_{PT} \gg (P_\uparrow)_{rad}$ starts. However, one has to pay attention to the vanishing behavior of Δn in the vicinity of the critical point and to its implication regarding the ball-lens effect. Equation (14) shows that d_1 becomes negative when $\Delta n < (\Delta n)_{min}$, a value below which the lensing disappears. For $a_0 = 2.2\ \mu$m, a numerical application gives $(\Delta n)_{min} = 9.2 \times 10^{-4}$ which is reached at $(T_C - T_0) = 3 \times 10^{-3}$ K. Since all our experiments were done for larger values of $(T_C - T_0)$, this condition is not relevant and a strong laser beam self-focusing is observed, as shown in Fig. 10 (case $T_C - T_0 = 0.6$ K).

If now we decrease the incident beam power from this situation, the droplets remain trapped. Indeed, their growth inside the beam induces a more and more efficient beam trapping. Moreover, the nuclei generated at the different intermediate beam waists continue to be trapped because of the strong intensity gradient existing at all these different foci. This irreversible trapping process is at the origin of the hysteretical behavior illustrated in Fig. 10.

3. *Crossover regime:* $(P_\uparrow)_{PT} \approx (P_\uparrow)_{rad}$

If we finally consider the case $H_N \approx H_P$, the hysteresis loop of a bulk ferromagnet is no longer square. As soon as $H > H_N$, nuclei develop. However, defects in the crystal structure, such as cavities, nonmagnetic inclusions, or internal stresses, lead inside the bulk to an irregular variation in H_P which cannot be neglected since $H_N \approx H_P$. A wall moves as long as it does not meet too important on obstacle. To overcome such a defect, it is necessary to increase the magnetic field in order to reach the associated value of H_P. Thus the domain grows until a new important obstacle is reached and so on. In this case the hysteresis loop presents the classical smooth variation. The behavior obtained for the self-focusing during the crossover regime $(P_\uparrow)_{PT} \approx (P_\uparrow)_{rad}$ is completely analogous. Up to now, we have always supposed there to be a dominant process, and we have always neglected disturbances like spherical aberrations induced on the wave by the droplets. However, during the crossover regime, these beam propagation "defects" are able to disturb nucleation and trapping in a noticeable way. Indeed, the efficiency of the ball-lens behavior of a droplet is related to its size, and because the droplet radius is limited by the beam radius, the transverse intensity distribution at a focus is strongly modified. Thus the nucleation dynamics

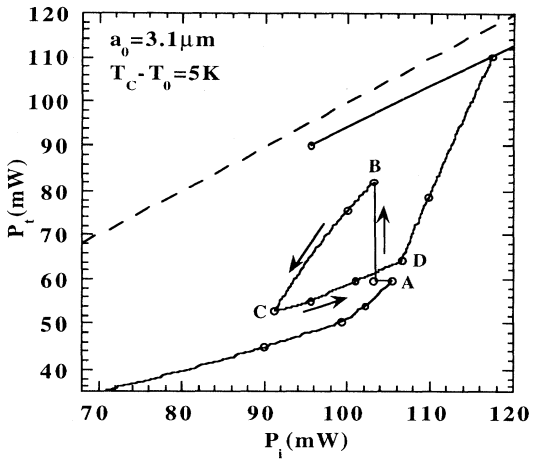

FIG. 11. Subloop in the case $(P_\uparrow)_{rad} \approx (P_\uparrow)_{PT}$. The arrows denote the stationary trajectory (except for point A from which P_i is slightly decreased before a complete stabilization of P_t) followed by P_t when varying P_i. Since point A is not recovered during the second incident beam power increase, return point memory does not hold in our system.

can be stopped by these large spherical aberrations. Nucleation of new droplets needs an incident beam power increase, and so on. The induced laser beam self-focusing is then more progressive as illustrated in Fig. 10 (case $T_C - T_0 = 4.5$ K) in which one can see the disappearance of a real self-focusing threshold. As shown in Fig. 11, the resulting smooth self-focusing allows the observation of hysteretical behaviors in partial cycling, observation which was impossible in the two above cases owing to the strong instability mechanism. At point A, the incident power is slightly decreased before a complete stabilization of the transmitted power. A partial instability mechanism is observed until point B, below which droplets are progressively detrapped, causing the transmitted power to follow the trajectory B-C. Then an incident power increase from point C leads to an increased trapping of the remaining droplets. Since the number of droplets in C is smaller than in B, the trajectory C-D is lower than B-C. At point D, the self-focusing follows the original path, just above point A. It seems therefore the return point memory effects [8,9] do not hold in our system, i.e., the ordered configuration of the metastable droplets is not preserved. The cycle creep phenomenon, analyzed at the end of this section, also evidences this property.

4. *Behavior of the system in* $P_\downarrow$

The behavior of the system in $P_\downarrow$ during the incident beam power decrease is completely symmetric to that in $P_\uparrow$. One has to consider "off-nucleation" and "off-propagation" fields $(P_\downarrow)_{PT}$ and $(P_\downarrow)_{rad}$ which obviously correspond, respectively, to the loss of thermodynamical stability and to the droplet detrapping. The expression of $(P_\downarrow)_{PT}$ is thus analogs to that of $(P_\uparrow)_{PT}$, but here, the minimum field-induced concentration variation required

for thermodynamical stability $(C_E)_C$ has to be replaced by $(C_1'-C_0)$. Therefore one gets

$$\frac{(P_\uparrow)_{PT}}{(P_\downarrow)_{PT}}=-\frac{(C_E)_C}{C_0-C_1'} . \tag{15}$$

At $(T_C-T_0)=6$ K, one finds $(P_\downarrow/P_\uparrow)=(P_\downarrow)_{PT}/(P_\uparrow)_{PT}=0.57$ in good agreement with the hysteresis loop illustrated in Fig. 6 from which we extract $(P_\downarrow)_{PT}/(P_\uparrow)_{PT}=0.60$.

Moreover, to define $(P_\downarrow)_{rad}$ we have to estimate the droplet volume corresponding to its detrapping. Since droplet growth is limited by the transverse intensity distribution, we approximate the largest droplet radius to the beam-waist value. Droplets of this size can no longer be considered as Rayleigh particles. The geometric optics regime $(2\pi r/\lambda \geq 100)$ is also irrelevant. At the present time, there is no analytical treatment in the case of Gaussian fields for our intermediate size regime. However, according to Ashkin [32], an order of magnitude of $(P_\downarrow)_{rad}$ can be given by trapping forces F calculated in terms of a nondimensional efficiency parameter Q from the expression

$$F=\sqrt{\varepsilon_L}\frac{QP_i}{c_1} . \tag{16}$$

Since trapping and detrapping thresholds result from the same optical force, one has

$$\frac{(P_\downarrow)_{rad}}{(P_\uparrow)_{rad}}=\frac{Q_\uparrow}{Q_\downarrow} , \tag{17}$$

where, according to experimental conditions, $Q_\uparrow=Q(r=r_c\approx 0.2\ \mu m)$ and $Q_\downarrow=Q(r=a_0=2.2\ \mu m)$. From [33] we get $(P_\downarrow)_{rad}/(P_\uparrow)_{rad}\approx 0.30$. This order of magnitude is within a factor of 2 smaller than that expected for hysteresis curves in the optical trapping regime. Experimentally we found values of $(P_\downarrow)_{rad}/(P_\uparrow)_{rad}$ between 0.5 and 0.6. However, the theoretical evaluation is very rough. Moreover, this discrepancy may be due to photophoresis [34], which was not taken into account. Finally, it is interesting to note that in all experiments, the measured values of $P_\downarrow$ as well as $P_\uparrow$ are beam-waist independent whatever the regime, as expected from Eqs. (8) and (12).

5. *Memory of the interaction: Limit hysteresis loop and cycle creep*

It has been noticed for a long time that the magnetization of bulk ferromagnets depends on the number of cycles, time, and stresses, but few experimental works have been devoted to these hysteretical behaviors. In particular, it is well known that successive hysteresis loops of a cyclically magnetized ferromagnet are not exactly reproducible. It was observed that loops of a verging domain structure usually stabilize after four or five cycles. This complicated phenomenon, discussed by Porteseil [17], results from an increasing organization of the domain structure during the successive cycles [35].

The hysteretical nature of the self-focusing generated by a laser-induced phase separation process must lead to the same behavior in the same kind of experiment. Figure 12 illustrates the expected irreversible evolution in the case $(P_\uparrow)_{PT}>(P_\uparrow)_{rad}$. The four hysteresis loops have been obtained consecutively according to the following procedure. After completely running the first loop until a return to $P_i=0$, a second lop is described, and so on. From Fig. 12 some important points have to be mentioned. First, it clearly confirms the hysteretical nature of the process; second, it illustrates the analogy with the magnetization of a ferromagnet; finally, it exhibits an important memory effect.

The strong decrease in $P_\uparrow$ during the second loop shows that the medium retains the memory of the interaction during the first cycle even if a linear propagation has been recovered below the $P_\downarrow$ value of this first loop. A macroscopic observation of the sample in the vicinity of the beam one hour after the completion of an experiment involving only one loop shows a large number of droplets already dispersed in the bulk. Moreover, according to the experimental procedure, the characteristic time necessary to decrease the incident beam power from $P_\downarrow$ to $P_i=0$ is of the order of a quarter of an hour. Thus a large number of droplets generated during the first loop are dispersed in the bulk when the second beam power increase occurs. Of course, owing to the slow thermodynamical destabilization outside the beam, the droplet radii are smaller than the beam waist which corresponds to the stationary droplet radius when the mixture is optically quenched. Unfortunately, we were not able to analyze this decrease of the droplet size with time and to describe the associated memory in a quantitatively way. Some qualitative characteristics can, however, be given.

The presence of these small droplets in the vicinity of the laser beam strongly modifies the different values of the thresholds $(P_\uparrow)_{PT}$ and $(P_\uparrow)_{rad}$ during the second beam power increase. At first, their existence decreases the nucleation barrier because they behave as heterogeneous nucleation centers. A decrease in $(P_\uparrow)_{PT}$ from the

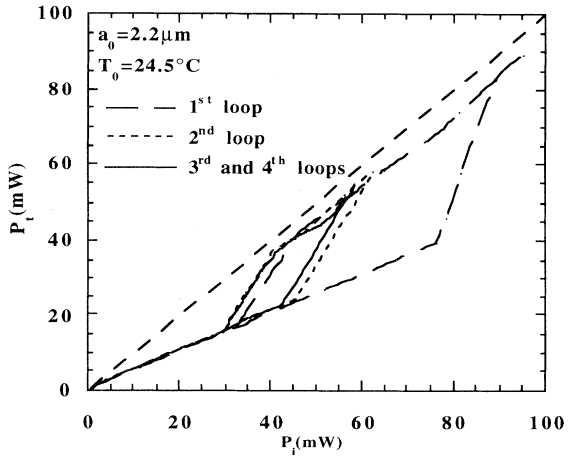

FIG. 12. Evolution of successive hysteresis loops and stabilization towards a limit cycle.

first to the second loop is then expected. Second, since the radius of these droplets is larger than the critical radius, the trapping threshold $(P_{\uparrow})_{\text{rad}}$ also decreases from the first to the second loop. Moreover, the decrease in $P_{\downarrow}$ from a loop to another is very small compared to that of $P_{\uparrow}$. This different behavior can be explained by the fact that the stationary droplet radius before detrapping (i.e., the beam radius) as well as the thermodynamical criterion of droplet stability (i.e., $|C_E| \geq |C_1' - C_0|$) are not significantly modified from loop to loop. However, as we shall specify later, the small decrease in $P_{\downarrow}$ should also be related to an increasing ordering of the set of beam-trapped droplets. Of course $P_{\uparrow}$ and $P_{\downarrow}$ reach limit values since nucleation and trapping are, respectively, limited by $|C_E| = |C_1' - C_0|$ and $r = a_0$.

Finally, we should mention a second general feature of the complicated behavior of hysteretical systems, particularly observed in polycrystal ferromagnets [36] and in superconductors [37]: cycle creep or reptation. When a ferromagnet is cycled dissymmetrically with respect to $H = 0$, the loops exhibit a slow positive drift towards increasing magnetization [38]. According to Néel [28], reptation is observed if three conditions are combined: (i) the existence of long-range couplings inside the domain structure, (ii) the existence of multiple domain configurations of close macroscopic energies, and (iii) the possibility for the system to switch from one configuration to another at random. As illustrated in Fig. 13, in submitting our sample to dissymmetrical increasing-decreasing variations of the incident beam power, when the beam is self-focused, an analogous behavior is observed: a laser beam self-focusing of increasing quality.

The Néel conditions for cycle creep have their analog in the optical situation. The long-range longitudinal couplings between droplets are generated by local intensity gradients induced by the ball-lens effect. Nucleation and growth processes provide the two final conditions. Many different droplet distributions along the beam axis can provide exactly the same transverse beam profile at the exit face of the cell, and therefore the same self-focusing response. Thus, as we predicted (and never evidenced) by Bloch during a discussion following a conference of Néel [39], the cycle creep phenomenon also appears in phase separating systems. Owing to the actual experimental limitations, we were not able to give a quantitative description of the optical cycle creep presented in Fig. 13. However, our experiment clearly shows that the droplet population adapts itself by selecting more and more ordered configurations since it has been generated by the wave. It also illustrates the universal character of the reptation phenomenon and shows that the return point memory property is not satisfied in our system.

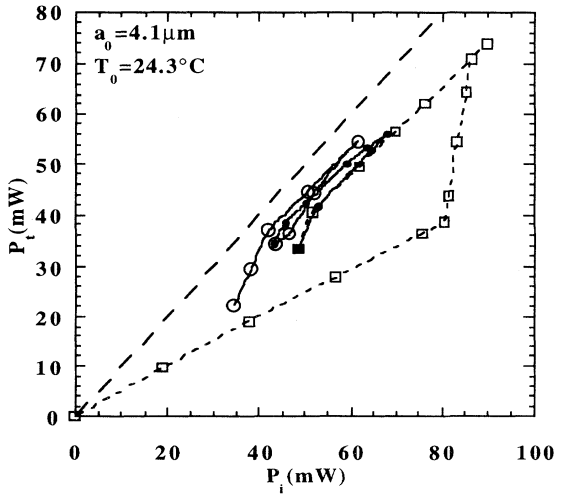

FIG. 13. Cycle creep phenomenon resulting from increasing-decreasing variations in P_i from a self-focused situation. It also demonstrates that return point memory does not exist in our system. The dashed line represents the variations in P_t when the diaphragm transmission equals one.

V. CONCLUSION

In this paper we have investigated the phenomenon of optical hysteresis in the case of a first-order phase transition resulting from laser-induced concentration variations in a binary liquid mixture. An experiment has been performed in a micellar phase of microemulsion located, in composition, in the vicinity of the liquid-liquid coexistence curve. First, we have theoretically described and experimentally analyzed the original laser-induced phase transition process. The type of involved interaction opens a new experimental thermodynamical path in the phase diagram, in order to manipulate mixtures and particularly to induce phase transitions. Besides temperature and pressure, the third thermodynamical variable, concentration, can also be externally monitored. In our particular medium, the induced quenching in composition was a thermodiffusive nature. To analyze the influence of the induced phase separation on the beam propagation, particular attention has been paid to the experimental configuration. When the thickness of the cell containing the sample is of the order of the beam perimeter, a stable cylinder composed of the minority phase is generated inside the beam. This cylinder behaves as an intrinsic bistable optical wave guide. In the more common situation where the sample is thick, such a cylinder is unstable. The morphology of the wave-medium system becomes completely different. Droplets are continuously nucleated in the beam. They are subsequently trapped by the wave, behave in their surrounding medium as bistable spherical lenses, and hysteretically self-focus the laser beam. Since it involves a one-dimensional geometry of interaction, this experiment illustrates very simply a Preisach scenario in the optical area. The lensing induces optical couplings between the droplets, each of them behaving as a bistable optical element of propagation.

Afterwards, we have experimentally analyzed such a scenario and compared the optical and magnetic processes. Our approach does not provide a universal description of hysteretical systems, but the comparison between two experiments as different as the laser propagation inside an optically quenched liquid mixture and the magne-

tization of a bulk solid ferromagnet gives an illustration sufficiently relevant to go thoroughly into a theoretical discussion of this subject, which is neither new nor solved.

One of the most important advantages of our one-dimensional geometry of interaction with respect to the Sixtus Tonks experiments concerns the ability to give a theoretical description of the fundamental processes, and to compare them with the measured one, which is difficult to achieve with bulk ferromagnets, owing to the large complexity of the domain structure. The agreement between predicted behaviors and experiments is quite satisfactory. Another advantage is the ability to precisely describe the influence, on the hysteresis loop, of the competition between the two processes associated with the phase separation and droplet trapping. The crossover regime, in which the thresholds are of the same order of magnitude, is particularly interesting according to a recent paper by Sethna *et al.* [40]. These authors propose a spin model for disorder-driven first-order phase transitions which includes interactions between domains and a random field acting on each of them to mimic their interactions with structural defects. This model, in which the shape of the hysteresis loops is driven by an instability mechanism disturbed by disorder, is particularly suitable for the description of our very simple geometry of interaction. Its adaptation to our situation is now in progress.

Moreover, to depict the complexity of hysteretical systems we have also analyzed other intrinsic behaviors often considered as secondary: a regime of asymptotic hysteresis when the sample is cycled after the first loop and the cycle creep phenomenon. As in ferromagnets, they are due to the complex domain structure induced by the wave-medium interactions. Even if, in the present experiment, we were only able to give a phenomenological description, the observed properties illustrate the value of optical hysteresis. Owing to the very simple geometry of the involved interaction, our experimental configuration provides interesting perspectives for improving the modeling of this difficult phenomenon. More generally, laser-induced first-order phase transition gives a new example of systems in which hysteretical behaviors appear very clearly. It also suggests that the associated irreversible and nonlinear phenomena, which deserve to be more deeply analyzed both experimentally and theoretically, should not be regarded as secondary statistical effects, but rather as general features to be considered when attempting to understand the fundamental properties of hysteretical systems.

ACKNOWLEDGMENTS

We are grateful to J. Plantard and M. Winckert for technical assistance. The Centre de Physique Moléculaire Optique et Hertzienne is "associé au Centre National de la Recherche Scientifique."

[1] D. A. B. Miller, J. Opt. Soc. Am. B **1**, 857 (1984).
[2] A. V. Kuznetsov, Opt. Commun. **81**, 106 (1991).
[3] P. Y. Wang, H. J. Zhang, and J. H. Dai, Opt. Lett. **13**, 479 (1988).
[4] I. Janossy, M. R. Taghizadeh, and E. Abraham, in *Optical Bistability III*, edited by H. M. Gibbs *et al.* (Springer-Verlag, Berlin, 1986).
[5] V. A. Stadnick, Opt. Commun. **68**, 445 (1988).
[6] F. Preisach, Z. Phys. **94**, 277 (1935).
[7] H. Ji and M. O. Robbins, Phys. Rev. B **46**, 14 519 (1992).
[8] J. Ortín, J. Appl. Phys. **71**, 1454 (1992).
[9] M. P. Lilly, P. T. Finley, and R. B. Hallock, Phys. Rev. Let. **71**, 4186 (1993).
[10] M. Giglio and A. Vendramini, Phys. Rev. Lett. **34**, 561 (1975); **38**, 26 (1977).
[11] A. J. Palmer, Opt. Lett. **5**, 54 (1980).
[12] B. Jean-Jean, E. Freysz, A. Ducasse, and B. Pouligny, Europhys. Lett. **7**, 219 (1988).
[13] E. Freysz, E. Laffon, J. P. Delville, and A. Ducasse, Phys. Rev. E **49**, 2141 (1994).
[14] J. P. Delville, C. Lalaude, E. Freysz, and A. Ducasse, Phys. Rev. E **49**, 4145 (1994).
[15] I. D. Mayergoyz, Phys. Rev. Lett. **56**, 1518 (1986).
[16] K. J. Sixtus and L. Tonks, Phys. Rev. **37**, 930 (1931); **42**, 419 (1932).
[17] J. P. Porteseil, Phys. Lett. A **121**, 145 (1987).
[18] L. Néel, C. R. Acad. Sci. **244**, 2668 (1957); L. P. Levy, J. Phys. (France) I **3**, 533 (1993).
[19] B. Jean-Jean, E. Freysz, A. Ponton, A. Ducasse, and B. Pouligny, Phys. Rev. A **39**, 5269 (1989).
[20] J. P. Gordon, C. C. Leite, R. S. Moore, S. P. S. Porto, and J. M. Whinnery, J. Appl. Phys. **36**, 3 (1965).
[21] J. D. Gunton, M. San Miguel, and P. S. Sahni, in *Phase Transition and Critical Phenomena*, edited by C. Domb and J. L. Lebowitz (Academic, New York, 1983), Vol. 8.
[22] D. Gazeau, E. Freysz, and A. M. Bellocq, Europhys. Lett. **9**, 833 (1989).
[23] L. Rayleigh, Philos. Mag. **34**, 145 (1882).
[24] E. F. Geodde and M. C. Yuen, J. Fluid Mech. **40**, 495 (1970).
[25] A. J. Liu, D. J. Durian, E. Herbolzheimer, and S. A. Safran, Phys. Rev. Lett. **65**, 1897 (1990).
[26] R. Y. Chiao, E. Garmire, and C. H. Townes, Phys. Rev. Lett. **13**, 479 (1964).
[27] L. D. Landau and E. M. Lifshitz, *Course of Theoretical Physics: Statistical Physics* (Pergamon Press, Oxford, 1958).
[28] L. Néel, J. Phys. Rad. **20**, 215 (1959).
[29] A. Herpin, *Théorie du Magnétisme* (Presses Universitaires de France, 1968).
[30] J. P. Delville, Ph.D. thesis, Université Bordeaux I, 1992 (unpublished).
[31] A. E. Siegman, *Lasers* (University Science Books, Mill Valley, CA, 1986).
[32] A. Ashkin, Biophys. J. **61**, 569 (1992).
[33] W. H. Wright, G. J. Sonek, and M. W. Berns, J. Appl.

Phys. **63**, 715 (1993).
[34] A. I. Sheifot and M. N. Gaidukov, Zh. Tekh. Fiz. **56**, 951 (1986) [Sov. Phys. Tech. Phys. **31**, 581 (1986)].
[35] J. L. Porteseil, J. C. Cotillard, and R. Vergne, J. Phys. (France) Lett. **39**, L-425 (1978).
[36] Nguyen Van Dang, J. Phys. Rad. **20**, 215 (1959).
[37] H. Rogolla and C. Heiden, Phys. Lett. **63A**, 63 (1977).
[38] J. L. Porteseil, Physica B **93**, 201 (1978), and references cited therein.
[39] L. Néel, in *Proceedings of the Robert A. Welch Foundation Conferences on Chemical Research. II. Atomic Structure* (Houston, TX, 1958), p. 167.
[40] J. P. Sethna, K. Dahmen, S. Kartha, J. A. Krumhausl, B. W. Roberts, and J. D. Shore, Phys. Rev. Lett. **70**, 3347 (1993).

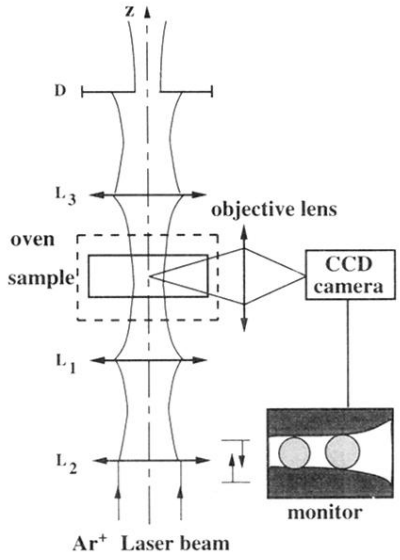

FIG. 2. Experimental setup.

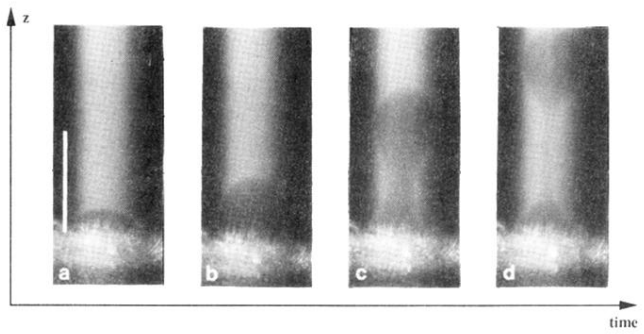

FIG. 3. Growth [(a), (b)] and hydrodynamic destabilization [(c), (d)] of a droplet nucleated heterogeneously at the internal entrance face of the cell containing the sample, when the optical path is large compared to the beam waist. z is the laser beam propagation axis. The control parameters are $1=2$ mm, $a_0=12$ μm, $P_i=240$ mW, $T_0=298$ K. The bar corresponds to 100 μm.

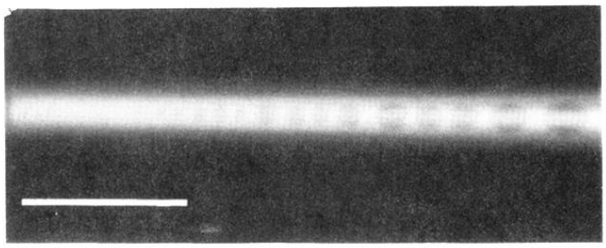

FIG. 4. Optical trapping of the droplets induced by the optical quench, and related laser beam self-focusing (essentially observed on the right part of the photograph). The left part corresponds to the entrance face of the cell. The control parameters are $l=2$ mm, $a_0=6$ μm, $P_i=220$ mW, $T_0=298$ K. The bar corresponds to 100 μm.

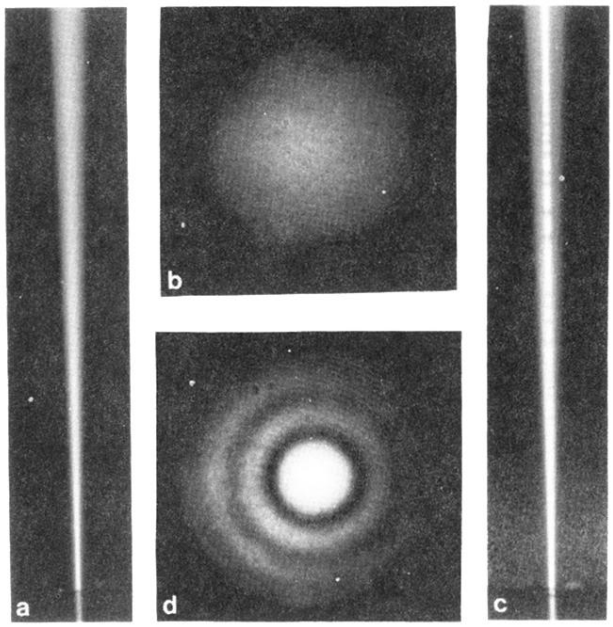

FIG. 7. Beam propagation and transverse beam profile below [(a), (b)] and above [(c), (d)] the self-focusing threshold $P_{\uparrow}$, at room temperature for $a_0 = 2.5$ μm. These photographs illustrate the beam propagation over one of the 2 mm of the cell length. (b) and (d) represent images of the transverse beam profile at the exit face of the cell. (a) and (b) show a classical linear propagation. (c) illustrates the laser beam self-focusing induced by the beam-trapped droplets generated by the optical quench in composition. The corresponding transverse beam profile (d) shows the intense beam spot resulting from this strong self-focusing process.

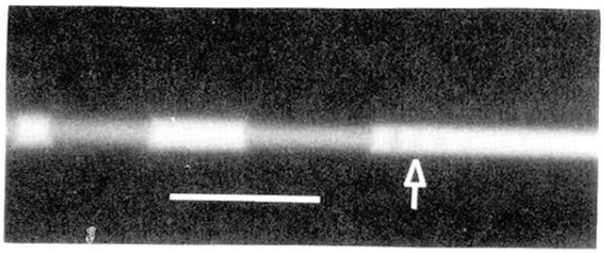

FIG. 9. Instability mechanism during the self-focusing process. A set of very small droplets (shown by the arrow) is induced at the intermediate beam waist resulting from the ball-lens behavior of the nearest beam-trapped droplet. The control parameters are $l=2$ mm, $a_0=6$ μm, $P_i=220$ mW, $T_0=298$ K. The bar corresponds to 50 μm.